Available online at www.sciencedirect.com
SCIENCE DIRECT®
International Journal of Heat and Mass Transfer 48 (2005) 3971–3981
International Journal of HEAT and MASS TRANSFER
www.elsevier.com/locate/ijhmt

Estimation of unknown outer-wall heat flux in turbulent circular pipe flow with conduction in the pipe wall

Cha'o-Kuang Chen *, Li-Wen Wu, Yue-Tzu Yang

Department of Mechanical Engineering, National Cheng Kung University, Tainan 70101, Taiwan, ROC

Received 25 September 2004; received in revised form 15 April 2005

Abstract

This study addresses the conjugate heat transfer problem of thermally developing, hydrodynamically developed turbulent flow in a circular pipe. An inverse method is used to estimate the unknown heat flux on the external surface of the circular pipe based on temperature measurements taken at several different locations within the fluid. The present approach rearranges the matrix forms of the governing differential equations, and then applies the linear least-squares-error method to determine the unknown boundary conditions of the pipe flow. The results confirm that the proposed method is capable of yielding accurate results even when errors in the temperature measurements are present, and that the accuracy of the estimated results is improved by taking temperature measurements in locations close to the inner-wall.

Keywords: Conduction; Convection; Heat transfer; Inverse; Numerical method; Turbulent; Pipe flow

1. Introduction

It is well-known that conjugate heat transfer, in which interaction occurs between the conduction effects in a solid wall and the convection effects within a fluid flowing around it, occurs in many engineering devices. A familiar example is that of a heat exchanger, in which there is an interaction between the conduction in the pipe wall and the convection in the fluid flowing over that wall. A further example of practical importance is the flow of a fluid over fins. In this case, valuable design information can be obtained by simultaneously analyzing the conduction in the fin and the convection in the fluid. A final significant example is that of the cooling rods within a nuclear reactor.

In the case of thin-walled pipes, the boundary conditions at the external surface are the same as those at the internal solid–fluid interface, and hence, early researchers neglected wall conduction effects and considered that the conditions on the external surface of the pipe also impose upon the surface of the inner-wall. However, for conjugate heat transfer in thick-walled pipes, the boundary conditions imposed at the external surface are different from those which exist at the internal surface. The problem of conjugate heat transfer has already been examined by a number of researchers [1–4]. Generally, these papers reveal that a substantial amount of heat transfer to the fluid can occur in the unheated sections of the pipe due to wall conduction effects. These effects are more pronounced when the solid-to-fluid thermal conductivity ratio k_{sf} is high and the inner-wall

* Corresponding author. Tel.: +886 6 275 7575; fax: +886 6 234 2081.
E-mail address: ckchen@mail.ncku.edu.tw (C.-K. Chen).

0017-9310/$ - see front matter © 2005 Elsevier Ltd. All rights reserved.
doi:10.1016/j.ijheatmasstransfer.2005.04.022

Nomenclature

A	constant matrix constructed from thermal properties and spatial coordinates
B	coefficient matrix of **C**
Bi	Biot number
C	vector constructed from the unknown boundary conditions
c_f	local friction coefficient
D	vector constructed from the boundary conditions
E	product of $\mathbf{A}^{-1}$ and **B**
F	error function
h	heat convection coefficient
k	thermal conductivity
L_d, L_c, L_u	lengths of the downstream, cooled and upstream sections
Pe	Peclet number
Pr	Prandtl number
q	heat flux on the outer-wall of the pipe
R	reverse matrix
r	radial coordinate
Re	Reynolds number
T	temperature vector
T	temperature
u	fluid axial velocity
u_τ	friction velocity
x	axial coordinate
y	distance from the wall

Greek symbols

α	thermal diffusivity
Δx	axial step size
Δr	radial step size
σ	standard deviation of the measurement error
v	kinematic viscosity
ω	random variable

Subscripts

exact	exact temperature
f	fluid
in	inlet
iw	inner-wall
i, *j*, *J*	indices
j_w	index of radial coordinate at inner-wall
m	mean
measured	measured temperature
ow	outer-wall
s	solid
t	turbulent

Superscript

$(\bar{})$	dimensionless quantity

radius ratio $\bar{r}_{iw} = r_{iw}/r_{ow}$ is low. In this situation, the thermal boundary conditions existing at the internal surface are not known a priori, and hence, the energy equations must be solved under the conditions of temperature and heat flux continuity.

Recently inverse heat conduction problems (IHCPs) have been analyzed for the situations where a direct measurement of the thermal boundary behavior is difficult, or indeed impossible, to carry out. Additionally, using direct measurement results to evaluate the heat loss in situations of this type is also very complex. Various analytical and numerical approaches have been proposed to overcome these technical limitations. For example, Chen and Lin [5] have presented a hybrid method of the Laplace transform technique and finite-difference method with a sequential in-time concept to estimate the unknown surface temperature of a plane plate in a two-dimensional IHCP using temperature measurements taken from within the plate. Furthermore, a method utilizing a boundary element inverse technique has also been developed for the estimation of local heat transfer coefficients on the surface of arbitrarily shaped solids [6]. Lin et al. [7] applied the finite-difference method with the linear least-squares-error method to estimate the thermal behaviors at the center and surface of a heated cylinder positioned normally to a turbulent air stream. Several researchers have also investigated the inverse problem related to the estimation of the thermophysical properties of a heat-conducting medium. Kim and Lee [8] focused on the estimation of the temperature-dependent thermal conductivity and volumetric heat capacity of a fluid flowing in a circular duct using the parameter estimation technique. Finally, Sawaf et al. [9] adopted an iterative procedure based upon minimizing the sum of squares function, and the Levenberg–Marquardt method, to estimate the linearly temperature-dependent thermal conductivity and specific heat capacity of an orthotropic solid.

Many researchers have used the temperature history and distribution within a fluid to determine the boundary conditions of the fluid flow. For example, Jian and Adriane [10] estimated the spatially non-uniform wall heat flux in a thermally developing hydrodynamically-developed turbulent flow in a circular pipe by means of finite element interpolation and the Levenberg–Marquardt method. Additionally, Park and Lee [11]

employed an inverse technique using the Karhunen–Loève Galerkin procedure to evaluate numerically the unknown functions of the wall heat flux for laminar flow inside a duct. Meanwhile, Bokar and Özisik [12] applied the conjugate gradient method of minimization with an adjoint equation to estimate the time-varying inlet temperature for laminar flow inside a parallel plate duct. Finally, Li and Yan [13] applied the same inverse method to estimate the space- and time-dependent wall heat flux for unsteady turbulent forced convection between parallel flat plates. However, these approaches all involved an iterative computational approach, and furthermore, they all neglected the effects of heat conduction within the wall in the vicinity of the solid–fluid interface.

The present study proposes an efficient technique which uses the linear least-squares-error method to estimate the unknown outer-wall heat flux for conjugate heat transfer within a thermally developing, hydrodynamically developed turbulent flow in a circular pipe. The proposed inverse method is used to solve the steady two-dimensional conduction equation for the pipe wall and the steady two-dimensional convection equation for the flowing fluid simultaneously. The method requires no prior knowledge of the functional form of the unknown wall heat flux, and yields solutions for the unknown conditions within a single computational iteration. The results confirm that the proposed method is capable of providing precise predictions of the unknown outer-wall temperature, and heat flux. As when using traditional IHCPs to solve unknown conditions (e.g. local heat flux, local Nusselt numbers, temperature, geometry, etc.), it is shown that the precision of the estimated results increases as the location of the temperature measuring points approaches that of the unknown quantities.

2. Physical model and governing equations

The present study considers a system in which a Newtonian fluid of constant properties flows with steady turbulent motion in a circular pipe. The fluid temperature at the inlet ($x = -L_u$) is assumed uniform and equal to T_{in}, and that the ambient air around the pipe is at a temperature of T_∞. As the fluid passes through the pipe, some of its heat is removed through the pipe wall via conduction. This results in an uncertain, spatially non-uniform, heat flux $\dot{q}(x)$ distribution along the surface of the outer-wall. In determining the values of this uncertain heat flux, the current study adopts the following simplifications:

1. Due to the symmetrical characteristics of the current problem, the domain need only consider one half of the pipe flow, and this flow can be assumed to be two-dimensional.

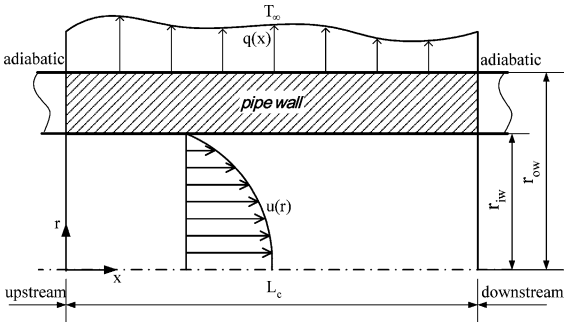

Fig. 1. System under consideration. Note that the velocity profile is fully developed and that the inlet temperature is constant. ($q(x)$ denotes the outer-wall heat flux function.)

2. The pipe wall is assumed to be homogeneous with a constant thermal conductivity, k_s. Furthermore, the wall has a finite thickness. The fluid is assumed to be incompressible, homogeneous, and to have a constant thermal conductivity, k_f.
3. An adiabatic condition is applied in the upstream region, i.e. $-L_u \leqslant x < 0$, and in the downstream region, i.e. $L_c < x \leqslant L_c + L_d$. Accordingly, the fluid and the pipe wall at $x = -L_u$ are assumed to of equal temperature, i.e. $T_s = T_f = T_{in}$.
4. The pipe length is such that a fully developed flow is established at the entrance and exit regions.

Fig. 1 presents a schematic representation of the considered pipe flow and conjugate heat transfer system. Meanwhile, Fig. 2 shows the detailed geometry, computational grid, and four types of measuring location considered in the present investigation.

The governing equations for the temperature field of the pipe flow can be expressed by the following differential equations:

In the wall region:

$$\frac{1}{r}\frac{\partial}{\partial r}\left(r\frac{\partial T(x,r)}{\partial r}\right)+\frac{\partial}{\partial x}\left(\frac{\partial T(x,r)}{\partial x}\right)=0 \tag{1a}$$

$$\text{at } x=-L_u \text{ and } r_{iw}\leqslant r\leqslant r_{ow},\quad T_s(x,r)=T_{in}=\text{const.} \tag{1b}$$

$$\text{at } r=r_{ow} \text{ and } 0\leqslant x\leqslant L_c,\quad \dot{q}(x) = -k_s\left(\frac{\partial T(x,r)}{\partial r}\right)_{r=r_{ow}}=h(T_{ow}(x,r_{ow})-T_\infty) \tag{1c}$$

In the fluid region:

$$u(r)\frac{\partial T(x,r)}{\partial x}-\frac{1}{r}\frac{\partial}{\partial r}\left[r(\alpha+\alpha_t)\frac{\partial T(x,r)}{\partial r}\right]=0 \tag{2a}$$

$$\text{at } x=-L_u \text{ and } 0\leqslant r\leqslant r_{iw},\quad T_f(x,r)=T_{in}=\text{const.} \tag{2b}$$

$$\text{at } r=0 \text{ and } -L_u\leqslant x\leqslant L_c+L_d,\quad \left(\frac{\partial T(x,r)}{\partial r}\right)_{r=0}=0 \tag{2c}$$

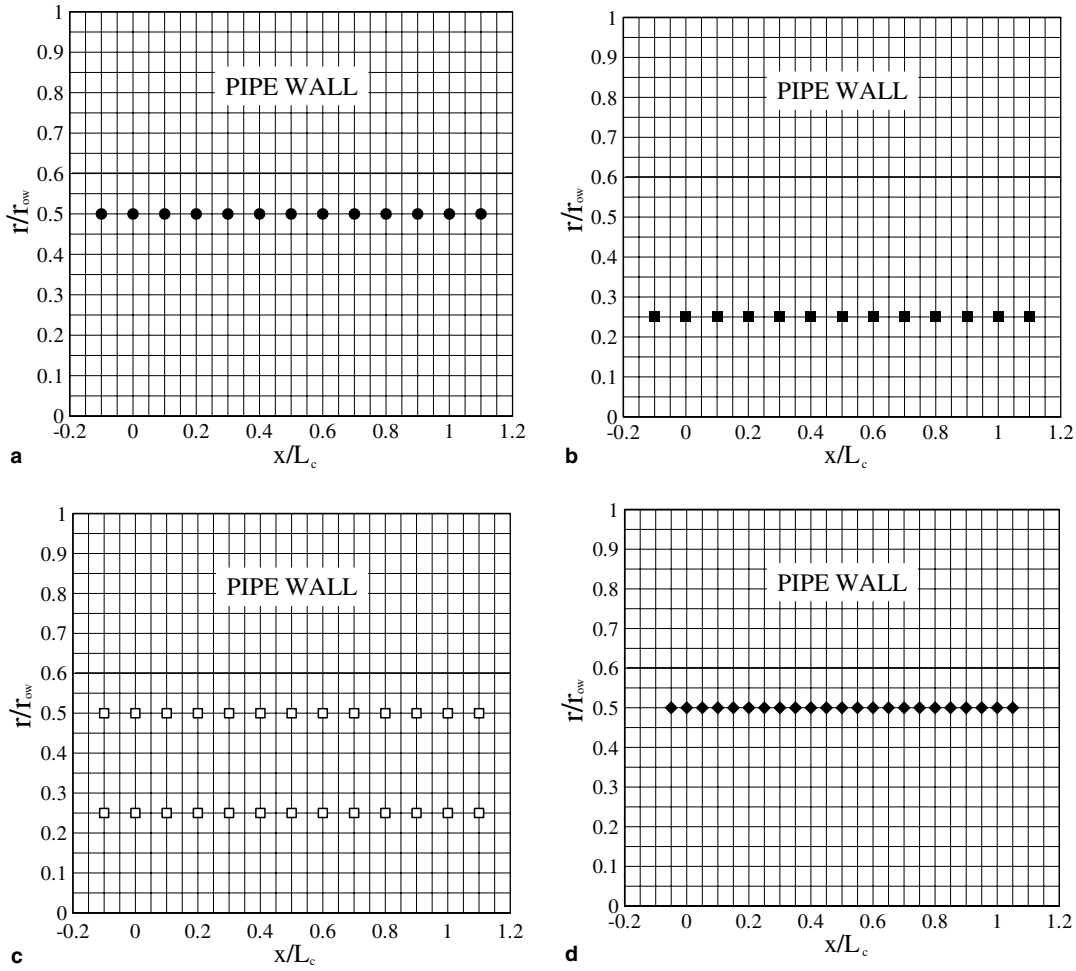

Fig. 2. Detailed dimensionless geometry and computational grid of a half domain of the pipe flow with three types of measuring point locations, i.e. (a) Type 1, (b) Type 2, (c) Type 3 and (d) Type 4.

At the interface between the pipe wall and the fluid inside the pipe ($r = r_{iw}$):

$$\partial T_f(x, r_{iw})/\partial r = k_{sf}\partial T_s(x, r_{iw})/\partial r \quad (3a)$$

$$T_s(x, r_{iw}) = T_f(x, r_{iw}) \quad (3b)$$

where r_{ow} and r_{iw} are the outer and inner pipe radii, respectively. The following parameters are defined: T_{ow} is the temperature on the external surface of the pipe, $\dot{q}(x)$ is the local heat flux on the external surface of the pipe, $u(r)$ is the hydrodynamically developed velocity profile, α is the thermal diffusivity, α_t is the turbulent thermal diffusivity, k is the thermal conductivity, and h is the heat-transfer coefficient.

The following scale factors are introduced to reduce the governing equations and the boundary conditions of Eqs. (1a)–(3b) to dimensionless forms, i.e.:

$$\bar{u} = \frac{u}{u_\tau}, \quad \overline{T} = \frac{T}{T_{in}}, \quad \bar{r} = \frac{r}{r_{ow}}, \quad \bar{x} = \frac{x}{L}, \quad \bar{q} = \frac{\dot{q} r_{ow}}{k_s T_{in}}$$

where $u_\tau = u_m\sqrt{c_f/2}$. The friction coefficient that fits the experimental data very well for $10^4 < Re < 5 \times 10^4$, $\frac{c_f}{2} = 0.039 Re^{-0.25}$, is substituted [14].

The governing parameters for conjugate conduction and turbulent forced convection heat transfer in the pipe subjected to non-uniform heat flux are the Reynolds number $Re_\tau = 2r_{iw}u_\tau/\nu$, the Prandtl number $Pr = \nu/\alpha$, the turbulent Prandtl number $Pr_t = \nu_t/\alpha_t$, the Biot number $Bi = hr_{ow}/k_s$, and the solid-to-fluid thermal conductivity ratio $k_{sf} = k_s/k_f$.

The fully developed velocity profile of turbulent flow of a Newtonian fluid in a circular pipe is obtained from the following expression for the dimensionless velocity in wall parameters [14],

$$\bar{u} = 2.5\ln\left[\bar{y}\frac{1.5(1+r/r_{iw})}{1+2(r/r_{iw})^2}\right] + 5.5 \tag{4}$$

where $\bar{y} = yu_\tau/v = (r_{iw}-r)u_\tau/v$.

The turbulent Peclet number Pe_t is given by the following expression,

$$Pe_t = \frac{v_t}{v}Pr \tag{5}$$

where $\frac{v_t}{v} = \frac{K\bar{y}}{6}\left(1+\frac{r}{r_{iw}}\right)\left[1+2\left(\frac{r}{r_{iw}}\right)^2\right]$. This equation is obtained from an empirical equation proposed by Reichardt [15]. And the Eq. (4) is developed from that with $K = 0.4$. The value of the Prandtl number Pr is taken to be 0.7. The turbulent Prandtl number Pr_t is given by the following expression, which fits well available experimental data [14],

$$Pr_t = \frac{1}{\frac{1}{2Pr_{t_\infty}} + CPe_t\sqrt{\frac{1}{Pr_{t_\infty}}} - (CPe_t)^2\left[1-\exp\left(-\frac{1}{CPe_t\sqrt{Pr_{t_\infty}}}\right)\right]} \tag{6}$$

where $C = 0.3$ and $Pr_{t_\infty} = 0.85$.

The number of independent dimensionless parameters in this problem is quite large. A parametric study of all individual parameters would require a vast set of results, and is not the principal objective of the present study. Hence, the values of certain dimensionless parameters are fixed, and just two heat transfer capability cases are examined, i.e. a low-Bi case with $Bi = 0.05$, $k_{sf} = 44.6$ and $Re = 2r_{iw}u_m/v = 3\times10^4$, and a high-$Bi$ case with $Bi = 0.1$, $k_{sf} = 44.6$ and $Re = 3\times10^4$.

The value of the dimensionless length of the cooled section, $\overline{L}_c = L_c/r_{ow}$, is specified as equal to 50, which is sufficiently long to observe the thermal development of the flow, while being sufficiently short to restrict the necessary computational effort to an acceptable level. Meanwhile, the dimensionless lengths of the upstream and downstream sections, $\overline{L}_u = L_u/r_{ow}$ and $\overline{L}_d = L_d/r_{ow}$, are set equal to $0.5\overline{L}_c$, which is long enough to account for the wall axial conduction effects and to ensure that the outlet boundary condition $(\partial\overline{T}/\partial\bar{x} = 0)$ is appropriate. The inner-wall radius ratio, $\bar{r}_{iw} = r_{iw}/r_{ow}$, is set equal to 0.6. Finally, the dimensionless ambient temperature is set equal to 0.1.

3. Numerical method

3.1. Direct problem

The present study employs the finite-difference method to analyze the direct problem. After discretization, the dimensionless governing equations and boundary conditions obtained from Eqs. (1a)–(2c) can be expressed in the following recursive forms:

In the wall region:

$$\frac{\overline{T}_{i,j+1}-2\overline{T}_{i,j}+\overline{T}_{i,j-1}}{(\Delta\bar{r})^2} + \frac{1}{\bar{r}_j}\frac{\overline{T}_{i,j+1}-\overline{T}_{i,j-1}}{2\Delta\bar{r}} + \frac{1}{\overline{L}_c^2}\cdot\frac{\overline{T}_{i+1,j}-2\overline{T}_{i,j}+\overline{T}_{i-1,j}}{(\Delta\bar{x})^2} = 0 \tag{7a}$$

$$\text{at } \bar{x} = -\frac{1}{2} \quad \text{and} \quad \bar{r}_{iw} \leqslant \bar{r} \leqslant 1, \quad \overline{T}_{0,j} = \overline{T}_{in} = 1 \tag{7b}$$

$$\text{at } \bar{r} = 1 \quad \text{and} \quad 0 \leqslant \bar{x} \leqslant 1, \quad \bar{q}_i = -\frac{\overline{T}_{i,J}-\overline{T}_{i,J-1}}{\Delta\bar{r}} = Bi\cdot\left(\overline{T}_{i,J}-\overline{T}_\infty\right) \tag{7c}$$

In the fluid region:

$$\frac{1}{2\bar{r}_{iw}\overline{L}_c}\cdot Re_\tau Pr\cdot\bar{u}_{i,j}\frac{\overline{T}_{i+1,j}-\overline{T}_{i-1,j}}{2\Delta\bar{x}} - \left(1+\frac{Pe_{t_j}}{Pr_{t_j}}\right)\left[\frac{\overline{T}_{i,j+1}-2\overline{T}_{i,j}+\overline{T}_{i,j-1}}{(\Delta\bar{r})^2}+\frac{1}{\bar{r}_j}\frac{\overline{T}_{i,j+1}-\overline{T}_{i,j-1}}{2\Delta\bar{r}}\right] = 0 \tag{8a}$$

$$\text{at } \bar{x} = -\frac{1}{2} \quad \text{and} \quad 0 \leqslant \bar{r} \leqslant \bar{r}_{iw}, \quad \overline{T}_{0,j} = \overline{T}_{in} = 1 \tag{8b}$$

$$\text{at } \bar{r} = 0 \quad \text{and} \quad -\frac{1}{2} \leqslant \bar{x} \leqslant \frac{3}{2}, \quad \frac{\overline{T}_{i,1}-\overline{T}_{i,0}}{\Delta\bar{r}} = 0 \tag{8c}$$

Substituting Eq. (3b) into the discretization equation obtained from the energy equation (Eq. (3a)) at the interface between the wall and the fluid inside the pipe gives the dimensionless inner-wall temperature as:

$$\overline{T}_{i,j_w} = \frac{k_{sf}}{k_{sf}+1}\overline{T}_{i,j_w+1} + \frac{1}{k_{sf}+1}\overline{T}_{i,j_w-1} \tag{9}$$

In Eqs.(7a)–(9) , $\Delta\bar{r}$ and $\Delta\bar{x}$ are the increments in the dimensionless spatial coordinates, $\overline{T}_{i,j}$ is the dimensionless temperature at the grid point (i,j), subscript i is the ith grid along the x-coordinate direction, subscript j is the jth grid along the r-coordinate direction, $\bar{q}_i$ is the dimensionless local heat flux on the outer-wall of the ith grid along the x-coordinate direction, subscript J represents the grid on the boundary $r = r_{ow}$, and subscript j_w represents the grid on the inner-wall, $r = r_{iw}$.

Regarding the treatment of the boundary conditions of Eq. (7c), the number of segments used on the boundary equals the number of nodes. Hence, the values of the dimensionless temperature, $\overline{T}_{i,J}$, at different nodes on the boundary can be treated as distinct. According to the inner-wall temperature expression given in Eq. (9), the dimensionless inner-wall temperature, $\overline{T}_{i,j_w}$, which is expressed by $\overline{T}_{i,j_w+1}$ at the first radial grid point in the pipe wall and by $\overline{T}_{i,j_w-1}$ at the last radial grid point in fluid, will be eliminated during algebraic vector manipulation. That is to say, the boundary conditions existing at the solid–fluid interface will be avoided, which significantly simplifies the subsequent analysis task.

As shown below, the heat conduction and convection equations can be combined to an equivalent matrix equation, which permits all of the unknowns to be

derived within a single computational iteration. Using the recursive forms an equivalent matrix equation for the direct analysis can be expressed as

$$\mathbf{A}_{n\times n}\mathbf{T}_{n\times 1} = \mathbf{D}_{n\times 1} \tag{10}$$

where matrix **A** is a constant matrix constructed from the thermal properties and spatial coordinates of the system. The components of vector **T** are the dimensionless temperatures at discrete points within the pipe wall and the fluid, while the components of matrix **D** are the functions of the dimensionless boundary conditions. The matrix elements of **A**, **T** and **D** are described in detail in Appendix A. The aim of the direct analysis process is to determine the dimensionless temperature at each node when all the boundary conditions and thermal properties are known. This is accomplished by using the Gauss elimination method to solve the direct problem expressed in Eq. (10) above.

In the present study, the dimensionless temperature data obtained from the direct problem are subsequently employed in the inverse problem to represent the measured temperature values of the fluid.

3.2. Inverse problem

The aim of the inverse problem is to determine the unknown thermal boundary conditions by using the temperature measurements taken from within the fluid in the pipe. Using the inner-wall temperature expression given in Eq. (9), the recursive forms of the governing equations given in Eqs. (7a) and (8a), and the boundary conditions given in Eqs. (7b), (7c), (8b) and (8c), can be rearranged in the form of a linear inverse model given by:

$$\mathbf{A}_{n\times n}\mathbf{T}_{n\times 1} = \mathbf{B}_{n\times m}\mathbf{C}_{m\times 1} \tag{11}$$

In the inverse analysis process, matrix **A** is constructed from known physical models and numerical methods, while vector **T** is composed of the temperature values measured by thermocouples at various locations within the fluid. Matrix **B** is the coefficient of vector **C**, which is composed of the unknown boundary conditions, including the inlet temperature and the temperatures, heat flux at discrete grid points along the external surface of the pipe. A major advantage of the proposed inverse approach is that the construction of the linear inverse model given in Eq. (11) requires no explicit assumptions regarding the functional forms of the unknown thermal quantities.

Finally, the temperature measurements are substituted into the inverse model of Eq. (11), which can then be solved using the following procedure:

Suppose that the estimated conditions of $\mathbf{C}_{\text{estimated}}$ can be obtained from the given estimated temperatures, $\mathbf{T}_{\text{estimated}}$, then:

$$\mathbf{A}\mathbf{T}_{\text{estimated}} = \mathbf{B}\mathbf{C}_{\text{estimated}} \tag{12}$$

Multiplying both sides by $\mathbf{A}^{-1}$ gives:

$$\mathbf{T}_{\text{estimated}} = \mathbf{A}^{-1}\mathbf{B}\mathbf{C}_{\text{estimated}} = \mathbf{E}\mathbf{C}_{\text{estimated}} \tag{13}$$

where $\mathbf{E} = \mathbf{A}^{-1}\mathbf{B}$.

Comparing the estimated temperatures, $\mathbf{T}_{\text{estimated}}$, with the measured temperatures, $\mathbf{T}_{\text{measured}}$, yields an error function, **F**, which can be represented as:

$$\mathbf{F} = (\mathbf{T}_{\text{estimated}} - \mathbf{T}_{\text{measured}})^{\mathrm{T}}(\mathbf{T}_{\text{estimated}} - \mathbf{T}_{\text{measured}}) \tag{14}$$

Substituting Eq. (13) into Eq. (14) gives the following matrix equation for this error function:

$$\begin{aligned}\mathbf{F} &= (\mathbf{E}\mathbf{C}_{\text{estimated}} - \mathbf{T}_{\text{measured}})^{\mathrm{T}}(\mathbf{E}\mathbf{C}_{\text{estimated}} - \mathbf{T}_{\text{measured}}) \\ &= \mathbf{C}^{\mathrm{T}}_{\text{estimated}}\mathbf{E}^{\mathrm{T}}\mathbf{E}\mathbf{C}_{\text{estimated}} - \mathbf{T}^{\mathrm{T}}_{\text{measured}}\mathbf{E}\mathbf{C}_{\text{estimated}} \\ &\quad - \mathbf{C}^{\mathrm{T}}_{\text{estimated}}\mathbf{E}^{\mathrm{T}}\mathbf{T}_{\text{measured}} + \mathbf{T}^{\mathrm{T}}_{\text{measured}}\mathbf{T}_{\text{measured}}\end{aligned} \tag{15}$$

This error function can then be minimized by differentiating **F** with respect to $\mathbf{C}_{\text{estimated}}$ as

$$\frac{\partial \mathbf{F}}{\partial \mathbf{C}_{\text{estimated}}} = 0 \tag{16}$$

Following a process of mathematical manipulation, it can be shown that:

$$\mathbf{E}^{\mathrm{T}}\mathbf{E}\mathbf{C}_{\text{estimated}} = \mathbf{E}^{\mathrm{T}}\mathbf{T}_{\text{measured}} \tag{17}$$

Hence, vector $\mathbf{C}_{\text{estimated}}$ can then be solved as follows:

$$\mathbf{C}_{\text{estimated}} = (\mathbf{E}^{\mathrm{T}}\mathbf{E})^{-1}\mathbf{E}^{\mathrm{T}}\mathbf{T}_{\text{measured}} = \mathbf{R}\mathbf{T}_{\text{measured}} \tag{18}$$

where $\mathbf{R} = (\mathbf{E}^{\mathrm{T}}\mathbf{E})^{-1}\mathbf{E}^{\mathrm{T}}$ is the reverse matrix of the unknown boundary conditions. The expressed process is derived by the least-squares-error method.

A common experimental approach is to measure only a few points when taking inverse problems. Therefore, when solving Eq. (18), it is only necessary to construct the parts of matrix $\mathbf{R}_{m\times n}$ and vector $\mathbf{T}_{n\times 1}$ which correspond to the measuring point locations in order to estimate the unknown boundary conditions of the problem. Consequently, the sizes of matrix $\mathbf{R}_{m\times n}$ and vector $\mathbf{T}_{n\times 1}$ reduce to $\mathbf{R}_{m\times n'}$ and $\mathbf{T}_{n'\times 1}$, respectively, where $n' < n$ and n' indicates the number of measuring points. It is obvious that the orders of the matrices are determined by the number of measuring points employed. In general, the accuracy of the estimated results is improved by selecting a larger number of measuring. However, this increases the computational and experimental costs, and hence, it is necessary to specify a number of measuring locations which yields an acceptable compromise between the precision of the results and the associated process costs.

In the present study, the inverse problem of Eq. (18) is solved by means of the linear least-squares-error method since this method removes the need for iterative computation, and enables the problem to be solved in a

linear domain. Furthermore, it can verify that the final solution of Eq. (18) from the proposed method is equivalent to the necessary condition of the optimum from the traditional non-linear least-squares approach [16–18]. Hence, the linear least-squares-error method can be used in place of the traditional non-linear least-squares approach, hence eliminating the requirement for an iterative process and an optimization phase when solving the inverse heat transfer problem.

A necessary and sufficient condition for Eq. (18) is that the rank of the reverse matrix **R** should be equal to the number of unknown variables. Therefore, it is necessary to specify a sufficient number of measuring points. In other words, if the rank of the reverse matrix **R** is less than the number of unknown elements of vector **C**, the number of measuring points must be increased.

4. Results and discussion

This paper considers the conjugate heat transfer case of hot fluid flowing through a pipe. Hence, the analyzed IHCP is one of heat conduction in the pipe wall on developing, turbulent forced convection flow and heat transfer inside the pipe. As the fluid flows through the pipe, heat is removed through the pipe walls via conduction, and is subsequently released to the environment. This paper analyzes the heat transfer by forced convection in internal turbulent flow which interacts with conduction in the pipe wall. The axial conduction of the pipe wall has a significant influence on both the upstream and downstream sections of the flow. In other words, the externally insulated segment of the pipe, located upstream or downstream of the cooled section, enables the fluid to release heat via axial conduction effects through the wall, and then releases this heat into the surrounding environment on the cooled section. The fluid is cooled both in the region $x < 0$ and in the region $x \geqslant 0$. Therefore, axial conduction reduces the maximum outer-wall temperature at the entrance of the cooled section ($x = 0$).

In order to investigate the relationship between the locations of the measuring points and the accuracy of the corresponding estimated results, four different types of measuring point locations are considered, as shown in Fig. 2. The sensors are located at the grid points marked in Fig. 2, while the dimensionless temperature data used in the simulation process are obtained from the solution to the direct problem.

In practice, the temperature measurements always contain some degree of error, whose magnitude depends upon the particular measuring method employed. Therefore, the simulated temperature measurements adopted in the current inverse problem are also considered to include measurement errors. For reasons of practicality, the present study adds a random error noise to the exact temperature values computed from the direct problem. Hence, the measured dimensionless temperature, $\overline{T}_{\text{measured}}$, is expressed as:

$$\overline{T}_{\text{measured}} = \overline{T}_{\text{exact}}(1 + \omega\sigma) \tag{19}$$

where $\overline{T}_{\text{exact}}$ is the exact dimensionless temperature, ω is a random variable generated by the DRNNOR subroutine of the IMSL [19], and σ is the standard deviation of the measurement error. For normally distributed random errors, the probability of a random value, ω, lying in the range $-2.576 < \omega < 2.576$ is 99% [20].

Fig. 3 presents a comparison between the predicted and the exact outer-wall temperatures for different types of measuring point location in the cases of $Bi = 0.05$ and $Bi = 0.1$. In general, the results reveal that for a measurement error of $\sigma = 1\%$, there is good agreement between the predicted and the exact results for Type 1 and Type 2 measuring locations. In IHCP problems, it is known that the precision of the estimated results is significantly influenced by the magnitude of the measurement errors. When measurement errors of $\sigma = 3\%$ and 5% are considered, it is noted that the errors in the estimated results

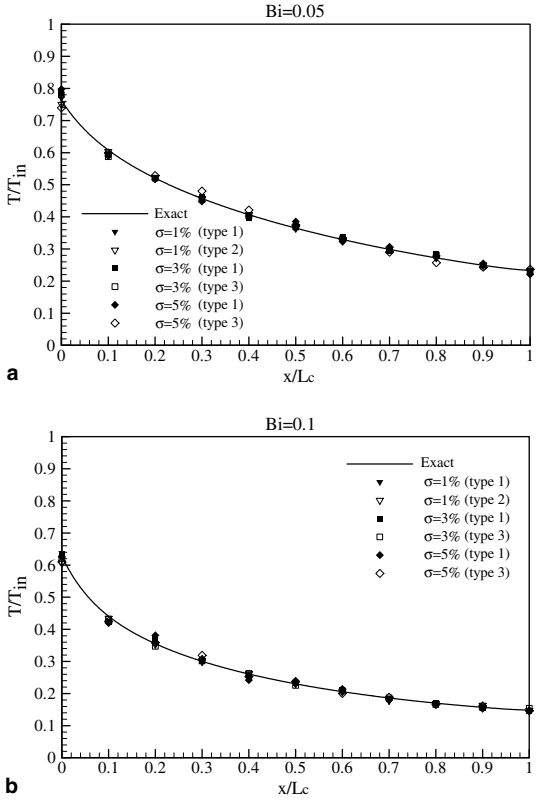

Fig. 3. Estimated dimensionless outer-wall temperature distributions for different types of measuring locations and measurement errors of $\sigma = 1\%$, 3% and 5% for the cases of: (a) $Bi = 0.05$ and (b) $Bi = 0.1$.

increase irrespective of which measuring point location type is specified, i.e. Type 1 or Type 2. Nevertheless, it can be observed that the results are still satisfactory. Considering the case where measurement errors of $\sigma = 3\%$ and $\sigma = 5\%$ are introduced, it can be seen that both sets of estimated results provide reasonable approximations to the exact solutions for Type 1 measuring point locations, but that the estimated results associated with a measurement error of $\sigma = 3\%$ are the more accurate. Consequently, it can be concluded that large measurement errors will degrade the performance of the proposed inverse method.

The present study also considers the relationship between the number of sensors employed and the accuracy of the estimated results. The results of Fig. 3 reveal that when measurement errors are considered, the accuracy of the results provided by the inverse method using Type 3 temperature measurements (i.e. 26 measuring points) is superior to that obtained using Type 1 (i.e. 13 measuring points). Therefore, it can be concluded that the use of more measuring points improves the performance of the proposed inverse method when the measured temperatures are subject to high measurement errors.

Fig. 4 presents a comparison between the estimated results and the exact solutions of the local dimensionless heat flux obtained using the three types of measuring point locations for measurement errors of $\sigma = 1\%$, $\sigma = 3\%$, and $\sigma = 5\%$ in the cases of $Bi = 0.05$ and $Bi = 0.1$. The results demonstrate that an increase in the Bi number increases the heat flux on the external surface of the pipe at its entrance. It is also observed that the accuracy of the estimated results decreases as the measurement error is increased. Furthermore, it is obvious that the estimations are accurate and robust when a measurement error $\sigma = 1\%$ is considered, and that the results are still satisfactory even when the measurement error increases to 3%. It indicates that the precision of the estimations depends strongly on the accuracy of the measurements in IHCP.

From the results of Fig. 4, it demonstrates that the estimated results associated with the Type 2 measuring point locations are inferior to those obtained from Type 1 and Type 3 measurements. This suggests that the precision of the inverse model is improved when the sensors are located closer to the surface whose unknown boundary conditions are to be determined.

Meanwhile, Fig. 5 shows that the proposed inverse method is still capable of yielding satisfactory results even when a measurement error ($\sigma = 5\%$) is introduced. The accuracy of the results provided by the inverse method using Type 4 temperature measurements is superior to that obtained using Type 3. This again confirms that the accuracy of the inverse method is improved when the sensors are located close to the solid–fluid interface, i.e. as the locations of the sensors approach

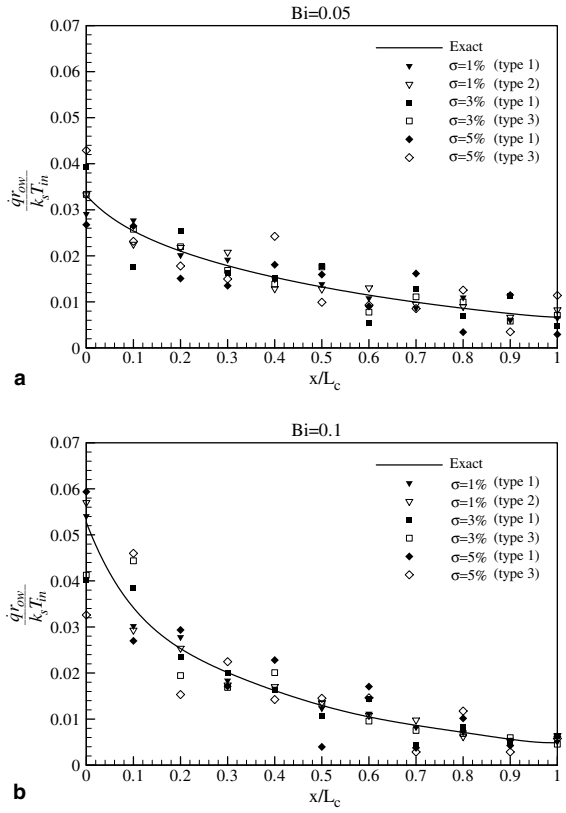

Fig. 4. Estimated dimensionless local heat flux distributions along the outer-wall for different types of measuring point locations with measurement errors of $\sigma = 1\%$, 3% and 5% for the cases of: (a) $Bi = 0.05$ and (b) $Bi = 0.1$.

the outer-wall whose unknown boundary conditions are to be predicted, the accuracy of the estimated results increases correspondingly.

The estimated distributions of Biot number with measurement errors $\sigma = 0\%$, $\sigma = 1\%$ and $\sigma = 3\%$ are shown in Fig. 6 for comparison, when the measuring location Type 1 is adopted. It reveals that the estimated and exact Biot number are in a very good agreement without considering measurement errors ($\sigma = 0\%$). Further, it is also obvious that the estimated results are accurate and robust when measurement error $\sigma = 1\%$ is included. When measurement error is $\sigma = 3\%$, the results are still satisfactory.

In a heating process, we could also solve an inverse conjugate heat transfer problem to estimate unknown outer-wall heat flux in a thermally developing, hydrodynamically developed turbulent flow in a circular pipe based on temperature measurements obtained at several different positions in the fluid. Fig. 7 considers the accuracy of the proposed method in estimating three different outer-wall heat flux functions estimated using Type

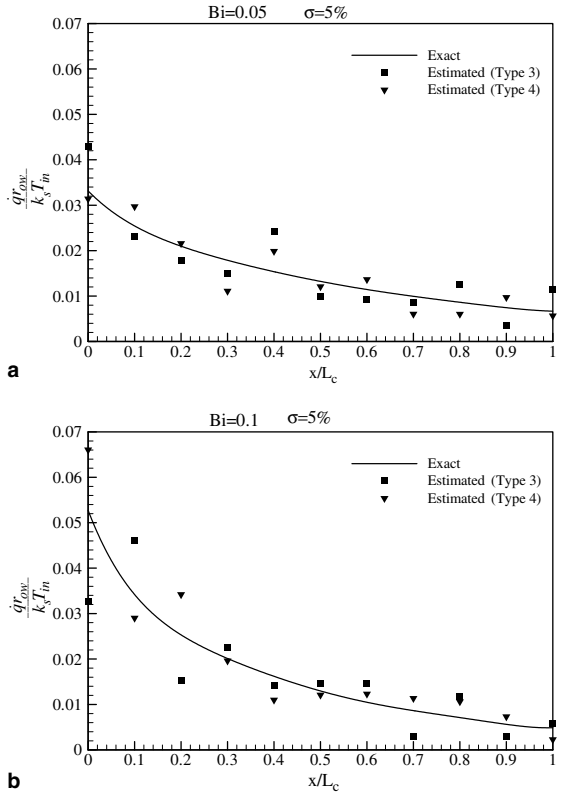

Fig. 5. Estimated dimensionless local heat flux distributions along the outer-wall with measurement errors of $\sigma = 5\%$ with Type 3 and Type 4 measuring point locations for the cases of: (a) $Bi = 0.05$ and (b) $Bi = 0.1$.

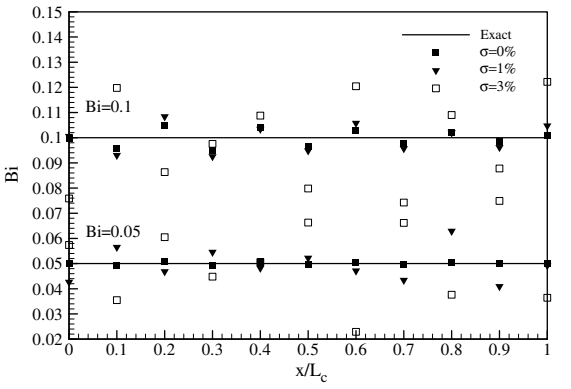

Fig. 6. Estimated distribution of Biot number along the outer-wall with measurement errors of $\sigma = 0\%$, 1% and 3% with Type 1 measuring point locations for the $Bi = 0.05$ and 0.1.

1 measuring point locations and measurement errors of $\sigma = 0\%$, $\sigma = 1\%$ and $\sigma = 3\%$. In the case where measurement errors are neglected, it can be seen that the esti-

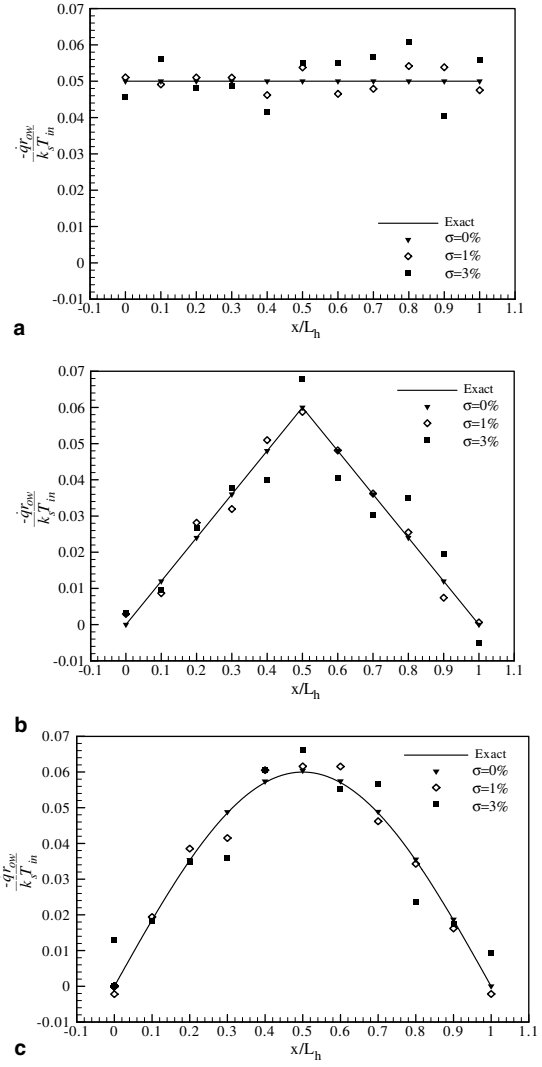

Fig. 7. Three test cases considered for outer-wall heat flux functions to examine the accuracy of inverse analysis with measurement errors of $\sigma = 0\%$, 1% and 3% with Type 1 measuring point locations, i.e. (a) uniform, (b) triangular ramp and (c) sine curve.

mated outer-wall heat flux distributions are in good agreement with the exact solutions for each of the three heat flux functions. Furthermore, it is confirmed that the estimated result exists and is unique through the verification of the proposed method. However, when measurement errors are considered, it is noted that there is a slight deviation between the estimated and exact solutions, and that the extent of this deviation is dependent upon the magnitude of the measurement errors. Consequently, the proposed inverse method is capable of yielding accurate results regardless of the magnitude of the outer-wall heat flux.

5. Conclusion

This paper has successfully applied an inverse method to the estimation of the unknown boundary conditions associated with turbulent flow of a hot fluid within a pipe. The influences of conduction effects within the pipe wall on the thermal development of the turbulent flow in a pipe with a finite heated/cooled length have been considered. The results of the inverse method can be derived within a single iteration, and demonstrate that the uniqueness of the solution can be easily identified. The proposed method has the further advantages that the unknown quantities of the thermal boundary conditions can be estimated directly, and that the inverse problem can be solved in a linear domain. It only takes about 9s of CPU time per computation. The CPU times correspond to a Intel Pentium 1 GHz processor, with 512MB RAM, running under the Microsoft Fortran PowerStation 4.0 platform.

The validity of the proposed method has been confirmed through the presentation of two test cases. In the first case, the heat flux to the environment in a cooling process has been presented for Biot numbers of 0.05 and 0.1, respectively. Therefore, the outer-wall heat flux of the pipe flow is an uncertain, spatially non-uniform distribution. In the second case, three outer-wall heat flux distributions in a heating process have been considered when estimating the outer-wall heat flux from the simulated measured temperature data. Since the proposed method does not require any information regarding the functional form of the outer-wall heat flux, the estimated results are seen to be more accurate and robust when the temperature measurement points are located closer to the boundary of interest, i.e. the outer-wall of the pipe in this case. The present results have revealed that the estimated results are accurate even when a measurement error of 3% is introduced. It has also been shown that the use of more measuring points within the fluid enhances the stability and accuracy of the estimated results when large measurement errors are present. In conclusion, the results have confirmed that the proposed inverse method is an accurate, robust, and efficient technique for solving the conjugate heat transfer problem associated with turbulent pipe flow.

Appendix A

We can rewrite Eqs. (7a) and (8a) in the following form:

$$a_j\overline{T}_{i,j} + b_j\overline{T}_{i+1,j} + c_j\overline{T}_{i-1,j} + d_j\overline{T}_{i,j+1} + e_j\overline{T}_{i,j-1} = 0$$

where a_j–e_j are the constant parameters constructed from the thermal properties and spatial coordinates of the system. And the equations can be expressed as a matrix model in linear algebra.

$$\mathbf{AT} = \mathbf{D} = \mathbf{BC}$$

where

$$\mathbf{A} = \begin{bmatrix} \overline{\mathbf{A}}_1 & \ddots & \ddots & & 0 \\ \ddots & \ddots & d_j\mathbf{I} & 0 & \\ \ddots & e_j\mathbf{I} & \overline{\mathbf{A}}_j & d_j\mathbf{I} & \ddots \\ & 0 & e_j\mathbf{I} & \ddots & \ddots \\ 0 & & \ddots & \ddots & \overline{\mathbf{A}}_J \end{bmatrix}_{I\cdot J\times I\cdot J},$$

$$\overline{\mathbf{A}}_j = \begin{bmatrix} \ddots & & \ddots & & 0 \\ \ddots & \ddots & \ddots & 0 & \\ \ddots & c_j & a_j & b_j & \ddots \\ & 0 & \ddots & \ddots & \ddots \\ 0 & & \ddots & & a_j + b_j \end{bmatrix}_{I\times I},$$

$$\overline{\mathbf{A}}_1 = \begin{bmatrix} \ddots & & \ddots & & 0 \\ \ddots & \ddots & \ddots & 0 & \\ \ddots & c_1 & a_1 + e_1 & b_1 & \ddots \\ & 0 & \ddots & \ddots & \ddots \\ 0 & & \ddots & & a_1 + e_1 + b_1 \end{bmatrix}_{I\times I},$$

$$\mathbf{T} = [\,\overline{\mathbf{T}}_1 \quad \cdots \quad \overline{\mathbf{T}}_j \quad \cdots \quad \overline{\mathbf{T}}_J\,]^{\mathrm{T}},$$

$$\overline{\mathbf{T}}_j = [\,\overline{T}_{1,j} \quad \cdots \quad \overline{T}_{i,j} \quad \cdots \quad \overline{T}_{I,j}\,]^{\mathrm{T}},$$

$\mathbf{I}$ is an identity matrix,

$$\mathbf{D} = [\,\overline{\mathbf{D}}_0 \quad \cdots \quad \overline{\mathbf{D}}_j \quad \cdots \quad \overline{\mathbf{D}}_J\,]^{\mathrm{T}},$$

$$\overline{\mathbf{D}}_j = \left[-c_j\overline{T}_{\mathrm{in}} \quad 0 \quad \cdots \quad \cdots \quad 0\right]^{\mathrm{T}}_{1\times I},$$

$$\overline{\mathbf{D}}_J = \left[-(c_J + d_J)\overline{T}_{\mathrm{in}} \quad -d_J\overline{T}_{i,J} \quad \cdots \quad \cdots \quad -d_J\overline{T}_{i,J}\right]^{\mathrm{T}}_{1\times I},$$

$$\mathbf{B} = \begin{bmatrix} \overline{\mathbf{B}}_0 \\ \vdots \\ \overline{\mathbf{B}}_j \\ \vdots \\ \overline{\mathbf{B}}_J \end{bmatrix}, \quad \overline{\mathbf{B}}_j = \begin{bmatrix} -c_j & & & & 0 \\ & 0 & & & \\ & & \ddots & & \\ & & & \ddots & \\ 0 & & & & 0 \end{bmatrix},$$

$$\overline{\mathbf{B}}_J = \begin{bmatrix} -(c_J + d_J) & & & & 0 \\ & -d_J & & & \\ & & \ddots & & \\ & & & \ddots & \\ 0 & & & & -d_J \end{bmatrix}$$

$\mathbf{C} = \left[\overline{T}_{\text{in}} \quad \overline{T}_{1,J} \quad \overline{T}_{2,J} \quad \cdots \quad \overline{T}_{I,J}\right]^{\text{T}}$. As above, the approximation model becomes linear combinations of the boundary conditions for the direct problem. Furthermore, it can lead to solving the inverse problem through the linear least squares error method.

References

[1] E.K. Zariffeh, H.M. Soliman, A.C. Trupp, The combined effects of wall and fluid axial conduction on laminar heat transfer in circular tubes, in: Proc. 7th Int. Heat Transfer Conf. Munich, Germany 4, 1982, pp. 131–136.

[2] S. Mori, M. Sakakibara, A. Tanimoto, Steady heat transfer to laminar flow in circular tube with conduction in the tube wall, Heat Transfer Jpn. Res. 3 (2) (1974) 37–46.

[3] M. Faghri, E.M. Sparrow, Simultaneous wall and fluid axial conduction in laminar pipe-flow heat transfer, ASME J. Heat Transfer 102 (1980) 58–63.

[4] A. Campo, C. Schuler, Heat transfer in laminar flow through circular tubes accounting for two-dimensional wall conduction, Int. J. Heat Mass Transfer 31 (1988) 2251–2259.

[5] H.T. Chen, S.Y. Lin, L.C. Fang, Estimation of surface temperature in two-dimensional inverse heat conduction problems, Int. J. Heat Mass Transfer 44 (2001) 1455–1463.

[6] T.J. Martin, G.S. Dulikavich, Inverse determination of steady heat convection coefficient distributions, ASME J. Heat Transfer 120 (1998) 328–334.

[7] J.H. Lin, C.K. Chen, Y.T. Yang, An inverse method for simultaneous estimation of the center and surface thermal behavior of a heated cylinder normal to a turbulent air stream, ASME J. Heat Transfer 124 (2002) 601–608.

[8] S.K. Kim, W.I. Lee, An inverse method for estimating thermophysical properties of fluid flowing in a circular duct, Int. Commun. Heat Mass Transfer 29 (8) (2002) 1029–1036.

[9] B. Sawaf, M.N. Özisik, Y. Jarny, An inverse analysis to estimate linearly temperature dependent thermal conductivity components and heat capacity of an orthotropic, Int. J. Heat Mass Transfer 38 (16) (1995) 3005–3010.

[10] J. Su, A.B. Lopes, Estimation of unknown wall heat flux in turbulent circular pipe flow, Int. Commun. Heat Mass Transfer 27 (7) (2000) 945–954.

[11] H.M. Park, J.H. Lee, A method of solving inverse convection problem by means of mode reduction, Chem. Eng. Sci. 53 (9) (1998) 1731–1744.

[12] J.C. Bokar, M.N. Özisik, An inverse analysis for estimating the time-varying inlet temperature in laminar flow inside a parallel plate duct, Int. J. Heat Mass Transfer 38 (1) (1995) 39–45.

[13] H.-Y. Li, W.-M. Yan, Identification of wall heat flux for turbulent forced convection by inverse analysis, Int. J. Heat Mass Transfer 46 (2003) 1041–1048.

[14] W.M. Kays, M.E. Crawford, Convective Heat and Mass Transfer, third ed., McGraw-Hill, New York, 1993, pp. 246–249.

[15] H. Reichardt, Arch. Ges. Warmetechnik 6–7 (1951) 129–143.

[16] R.E. Kalman, A new approach to linear filtering and prediction problems, Trans. ASME 82D (1990) 35–45.

[17] H.W. Sorenson, Parameter Estimation: Principles and Problems, Marcel Dekker, New York, 1980.

[18] C.Y. Yang, Noniterative solution of inverse heat conduction problems in one dimension, Commun. Numer. Meth. Eng. 13 (6) (1997) 419–427.

[19] IMSL User's Manual, 1985, Math Library Version 1.0, IMSL Library Edition 10.0, IMSL, Houston, TX.

[20] A.J. Silva Neto, M.N. Özisik, Inverse problem of simultaneously estimating the timewise varying strength of two-plane heat source, J. Appl. Phys. 73 (1993) 2132–2137.